International Journal of Microwave and Wireless Technologies

cambridge.org/mrf

CPW-fed concurrent, dual band planar antenna for millimeter wave applications

Smriti Agarwal[1] and Dharmendra Singh[2]

[1]Department of Electronics and Communication Engineering, Govind Ballabh Pant Government Engineering College, New Delhi 110020, India and [2]Department of Electronics and Communication Engineering, Indian Institute of Technology Roorkee, Roorkee 247667, India

Research Paper

Cite this article: Agarwal S, Singh D (2018). CPW-fed concurrent, dual band planar antenna for millimeter wave applications. *International Journal of Microwave and Wireless Technologies* **10**, 1088–1095. https://doi.org/10.1017/S1759078718001009

Received: 26 November 2017
Revised: 27 May 2018
Accepted: 29 May 2018
First published online: 4 July 2018

Key words:
Antenna design; modeling and measurements; RF front-ends

Author for correspondence:
Smriti Agarwal, E-mail: smritiagarwal@gbpec.edu.in

Abstract

In recent years, millimeter wave (MMW) has received tremendous interest among researchers, which offers systems with high data rate communication, portability, and finer resolution. The design of the antenna at MMWs is challenging as it suffers from fabrication and measurement complexities due to associated smaller dimensions. Current state-of-the-art MMW dual-band antenna techniques demand high precision fabrication, which increases the overall cost of the system. Henceforth, the design of an MMW antenna with fabrication and measurement simplicity is quite challenging. In this paper, a simple coplanar waveguide (CPW) fed single-band MMW antenna operating at 94 GHz (W band) and a dual-band MMW antenna operating concurrently at 60 GHz (V band) and 86 GHz (E band) have been designed, fabricated, and measured. A 50 Ω CPW-to-microstrip transition has also been designed to facilitate probe measurement compatibility and to provide proper feeding to the antenna. The fabricated single frequency 94 GHz antenna shows a fractional bandwidth of 11.2% and *E*-plane (*H*-plane) gain 6.17 dBi (6.2 dBi). Furthermore, the designed MMW dual-band antenna shows fractional bandwidth: 2/6.4%, and *E*-plane (*H*-plane) gain: 7.29 dBi (7.36 dBi)/8.73 dBi (8.68 dBi) at 60/86 GHz, respectively. The proposed antenna provides a simple and cost-effective solution for different MMW applications.

Introduction

Growing demand for high data rate wireless applications and overflooded traffic at microwave frequency has surged the research in millimeter wave (MMW) band (30–300 GHz). The wide bandwidth of 7 GHz (57–64 GHz) centered around 60 GHz (V band) is available for unlicensed wireless communication, although, its range is limited to few kilometers due to the strong atmospheric absorption 15–30 dB/km depending on the atmospheric conditions [1]. Also, 71–88 GHz (E band) and 94 GHz (W band) find applications in point to point high data rate communications and standoff imaging application for security screening, respectively. Moreover, MMWs offer portable, light weight systems and good frequency reuse capability in contrast to their microwave counterparts [2, 3]. MMW antennas, which are an indispensable element of any transceiver system, exhibit several design challenges such as limited gain, complex structure, higher order mode losses, unavailability of transmission line model, etc. [4]. Hence, in this paper, an MMW antenna with optimum features has been aimed to design.

Furthermore, the planar antenna is a natural choice for radio frequency (RF) frontend due to its compactness, conformity, integrability, and ease of fabrication. Increasing demand for miniaturized and multi-tasking communication devices has excelled the design of dual-band RF systems and hence there is a need for a dual resonant MMW antenna structure that provides concurrency as well as redundancy. The current state-of-the-art dual-frequency antenna discusses various techniques mainly in the microwave frequency band, such as reactive loading by placing shorting pins, slots, stubs, spur, notch, etc. at appropriate locations in the patch that excites dual resonance with varying frequency ratios depending on their relative positions [5], multiple coplanar/stacked patch providing same or dual polarization [6], artificially structured metamaterials such as split-ring resonator (SRR), which offers high-quality factor [7]. However, the dual-band antenna at the MMW frequency is still very less explored. Few of the reported works are: 58/77 GHz antenna using flip-chip assembly [8], fractal bowtie antenna using movable plate for 60/77 GHz [9], 40/60 GHz SRR-based antenna [10], and 24/60 GHz antenna using the 0.1 μm standard complementary metal-oxide semiconductor (CMOS) process [11]. Most of these reported MMW dual-band antenna techniques require sophisticated fabrication techniques/equipment and high level of precision which makes them complex and cost inefficient. Thereby, there is a great need for research in this important area.

CAMBRIDGE UNIVERSITY PRESS

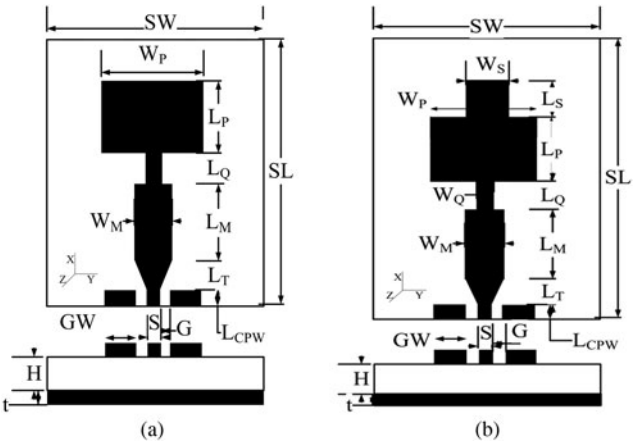

Fig. 1. CPW-fed millimeter wave antenna geometry of (a) single frequency 94 GHz and (b) dual frequency 60/86 GHz (dimensions not to scale).

Keeping in account these prerequisites a single layer, simple, compact, and conformable antenna structure is aimed to be designed. In this paper, a single-frequency (94 GHz) and a dual-frequency (60/86 GHz) millimeter wave microstrip antennas have been designed. Moreover, in order to facilitate measurement of the fabricated prototype antenna using a ground-signal-ground (GSG) probe, a wideband CPW to microstrip transition has also been designed. The paper is divided into the following sections: section "MMW antenna design challenges" deals with antenna design challenges, section "MMW antenna modeling approach" discusses modeling approach of the proposed millimeter wave antenna, sections "Parametric variation of stub dimensions" and "Surface current distribution on antenna" cover parametric variations and surface current distribution, respectively. MMW antenna fabrication and measurement procedure are given in sections "MMW antenna fabrication" and "antenna measurement setup". Finally, results are discussed in the section "Results and discussion" and concluded in section "Conclusion".

MMW antenna design challenges

There are several practical challenges which need to be undertaken while designing an antenna at MMW frequency with good performance, like:

Choice of suitable substrate

At the MMW, transverse electric (TE) and transverse magnetic (TM) surface waves are more likely to be excited on a grounded substrate and reduce the radiation efficiency. The cut-off frequency of these modes is given by [12]:

$$f_c = \frac{nc}{4h}\sqrt{(\varepsilon_r - 1)}, \tag{1}$$

where c is the speed of light, h is the height of substrate, $n = 0, 1, 2, 3,\ldots$ for TM0, TE1, TM2, TE3,… surface modes. Thereby, a suitable substrate is needed to be chosen for MMW antenna design such that cut-off frequency of higher order mode is well above the operating frequency.

Probe measurement feasibility

At MMW frequency, antenna prototypes are commonly tested using probe measurement [13]. In order to be compatible with the available GSG probe, a coplanar transmission line of 50 Ω characteristic impedance is needed to be designed operating in the fundamental CPW mode.

CPW to microstrip transition

In order to couple maximum RF power from CPW feed to the radiating patch, a CPW-to-microstrip transition is needed to be designed with low insertion loss and covering the full frequency range of interest [14].

Fabrication constraint

To achieve dual resonance, at MMW frequency commonly used techniques, such as, cutting slots, closely placed multiple patches, metamaterials, etc. need stringent fabrication and alignment accuracies (due to the correspondingly low $\lambda/2 \approx 1.5$–2.5 mm), so a relatively simple and efficient technique is needed to be used without complicating the fabrication procedure or raising the cost.

MMW antenna modeling approach

The modeling approach of the proposed MMW antenna can be described by distributing the antenna design into three constituent parts: (1) antenna feed section, (2) transition section, and (3) radiating patch. Simulation of each of the antenna section has been done using 3D full-wave EM solver HFSS which is based on the finite-element method technique. The detailed description of each of the antenna section is as follows:

Antenna feed section

The efficient on-wafer characterization of MMW prototype circuit requires coplanar (G–S–G) probe testing for the reason of convenience and because of having ground and signal on the same plane [13, 15]. For this, firstly, a 50 Ω CPW feedline is designed which is integrated on the same substrate as shown in Fig. 1. Since a microstrip antenna consists of a ground plane below the substrate to suppress any backward radiation. Thereby, CPW design considered is the conductor backed-CPW (CBCPW). The upper limit of normalized side ground plane width (GW/(S + 2G)) is approximately $\lambda_g/8$ to keep the radiation losses and dispersion small while the lower limit is twice the conductor width (S) to reduce attenuation due to the conductor losses of the signal line [16]. The limiting frequency corresponds to the frequency where phase constants of the CPW mode and the first lateral higher order mode intersect beyond which it shows highly dispersive behavior. These higher order modes depend on both lateral line dimensions(W_{tot}) and substrate thickness H and given by [17]:

$$f_g(W_{tot}) = \frac{2}{W_{tot}\sqrt{2\mu_0\varepsilon_0(\varepsilon_r - 1)}}, \tag{2}$$

where $W_{tot} = S + 2G + 2GW$,

$$f_g(h) = \frac{1}{H \cdot \sqrt{\mu_0\varepsilon_0(\varepsilon_r - 1)}}. \tag{3}$$

https://doi.org/10.1017/S1759078718001009 Published online by Cambridge University Press

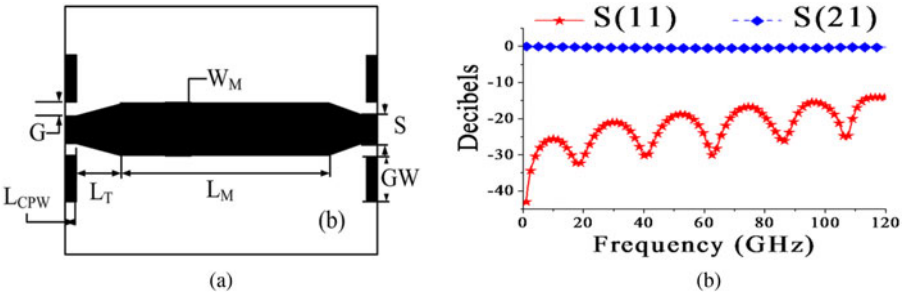

Fig. 2. A back-to-back transition of finite-ground conductor backed CPW (FG-CBCPW) to microstrip transmission line: (a) geometric structure and (b) simulated *S*-parameter plot.

A finite width-CBCPW (FW-CBCPW) resembles a system of three coupled microstrip lines (MSLs). So, the length of FW-CBCPW should be kept much less than the half wavelength of MSL mode, i.e. $L \ll (\lambda_0/\sqrt{\varepsilon_r})/2$ to avoid excessive cross-talk or possible resonance [18]. So, keeping in view of these limitations for single CPW mode propagation, and dimensional constraints of the available GSG probe pitch of 150 µm, the simulated dimensions of the 50 Ω FG-CBCPW line comes out to be GW/G/S = 0.4 mm/0.03 mm/0.2 mm as shown in Fig. 2(a).

Transition section (coplanar waveguide (CWP) to microstrip transition)

In order to facilitate measurement of microstrip-based structures through coplanar probes, a coplanar to microstrip transition is required [14]. Therefore, a good matching transition is needed in order to effectively propagate the RF signal from coplanar feed to the antenna. The width of the simulated 50 Ω MSL comes out to be $W_M = 0.38$ mm. Now, since the width of the 50 Ω MSL and 50 Ω FG-CBCPW line are not same; hence, a transition structure is required such that to avoid any mismatch between the MSL and CPW lines. Primarily, there are two types of transitions, one that uses via hole and second type uses vialess transition. Via hole, however, provides broadband transition but adds complexities in fabrication [19]. Therefore, via less transition was preferably used. Here, a smooth taper connects the center conductor of CPW line to the MSL which provides a gradual change in field and impedance, minimizing overall reflection and maximizing the transmission as shown in Fig. 2(b). The length of transition is approximately $\lambda_g/4$ long at the center frequency of operation, i.e. $f_1 + (f_2 - f_1)/2$, where λ_g is the guided wavelength [13]. Apart from transition region length, the bandwidth of CPW-to-microstrip transition also depends on CPW feed-line length due to the propagation of coplanar microstrip mode along the CPW feed line [19]. Hereby, by keeping CPW pad length low enough a wide bandwidth CPW-to-microstrip transition was achieved covering the upper MMW frequency limit of our interest as shown in Fig. 2(b). The designed transition is compact, wide band and vialess, hence, makes the fabrication process relatively less expensive and less complicated.

Radiating patch section

The initial structure of the antenna is a rectangular microstrip patch. The resonant frequency of this microstrip patch antenna depends upon its resonant dimension and is given by [20]:

$$f_r = \frac{c}{2\sqrt{\varepsilon_r}}\sqrt{\left(\frac{m}{L_e}\right)^2 + \left(\frac{n}{W_e}\right)^2}, \tag{4}$$

where L_e is the effective length and W_e is the effective width taking into account fringing field effect. The geometry of the simulated single-band MMW planar antenna is shown in Fig. 1(a). The patch radiator is fed through the 50 Ω MSL via a quarter wave matching network. Here, instead of probe feeding, inline microstrip feeding has been used as a coaxial probe pin at the MMW band is approximate of the same cross-section as of the MMW planar antenna. So, it is practically infeasible to drill a hole to provide a proper contact between the two, i.e. antenna and the feed. The other end of the MSL is terminated to the 50 Ω finite ground CBCPW (FG-CBCPW) line through the microstrip to CPW taper transition in order to facilitate measurement using the GSG probe.

Next, the geometry of the simulated dual-band MMW planar antenna is shown in Fig. 1(b). One of the techniques for obtaining tunability to the microstip antenna is adding a stub [21–24]. Hence, in order to obtain dual-band effect reactive loading of the patch has been done by using an open-circuit stub. Input impedance (Z_{oc}) of open-circuit stub ($Z_L = \infty$, Z_0 = stub impedance = Z_{stub}, l = length of stub (L_s), β = propagation constant) is given by

$$Z_{oc} = Z_0\frac{Z_L + jZ_0\tan(\beta l)}{Z_0 + jZ_L\tan(\beta l)} = -jZ_{stub}\cot(\beta l). \tag{5}$$

Thus, the input impedance of the open-circuited stub is capacitive or inductive around the resonance frequency of the patch [21, 25]. For a given stub impedance (Z_{stub}), stub width (W_s) can be found by the standard microstrip formula [25] as follows:

$$\frac{W_s}{h} = \begin{cases} \dfrac{8e^A}{e^{2A}-2} & (W_s/h) < 2, \\ \dfrac{2}{\pi}\left[B - 1 - \ln(2B-1) + \dfrac{\varepsilon_r - 1}{2\varepsilon_r}\left\{\ln(B-1) + 0.39 - \dfrac{0.61}{\varepsilon_r}\right\}\right] & (W_s/h) > 2, \end{cases} \tag{6}$$

https://doi.org/10.1017/S1759078718001009 Published online by Cambridge University Press

Table 1. Final optimized dimensions of single- and dual-frequency MMW antennas

Parameters (mm)	L_P	W_P	L_Q	W_Q	L_M	W_M	L_T	L_{CPW}	L_S	W_S
Single-freq. antenna	0.95	1.44	0.48	0.1	0.86	0.38	0.45	0.1	–	–
Dual-freq. antenna	1.25	2	0.6	0.1	0.94	0.38	0.3	0.1	0.48	0.5

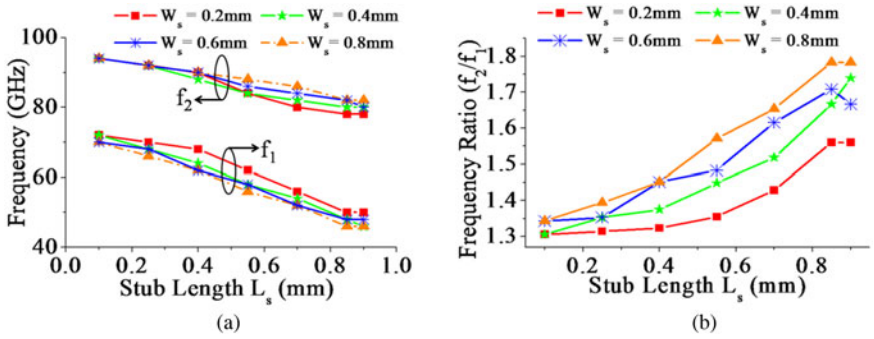

Fig. 3. Effect of varying stub length (L_s) and stub width (W_s) on (a) the two dual resonant frequencies f_1 and f_2 and (b) on the frequency ratio (f_2/f_1) characteristic.

where

$$A = \frac{Z_{stub}}{60}\sqrt{\frac{\varepsilon_r + 1}{2}} + \frac{\varepsilon_r - 1}{\varepsilon_r + 1}\left(0.23 + \frac{0.11}{\varepsilon_r}\right) B = \frac{377\pi}{2Z_{stub}\sqrt{\varepsilon_r}}.$$

When the length of the stub is small, it yields tunability, whereas when it is comparable with $\lambda/4$ ($\beta l = \Pi/2$), it excites other higher order mode (TM_{11}) resonant frequency and yields dual-frequency operation [26]. Thereby, as shown in Fig. 1(b), an open circuited $\lambda/4$ stub at the radiating edge of the patch has been placed in order to achieve the MMW dual-band antenna. The short-circuit stub was not used due to the complexities in shorting the stub to the ground.

The composite MMW antenna structure (CPW feed + CPW to microstrip transition + radiating patch) for a single frequency (94 GHz) and dual frequency (60/86 GHz) was simulated and optimized using HFSS. The final dimensions were obtained using sequential nonlinear programming optimization technique available in HFSS. The dimensions of the two proposed MMW antennas are given in Table 1. Here, the nomenclature used of different parameters can be found in Fig. 1. The cross-sectional area of single- and dual-frequency antennas is 2.9 & 3.7 mm^2, respectively.

Parametric variation of stub dimensions

With the help of parametric variations of stub length (L_s) and stub width (W_s), their effect on antenna dual resonance has been investigated. On varying the stub length, it was observed that the stub modifies the fundamental and higher order mode resonance frequencies of the patch and thereby, realizing dual response. The variation in the two resonant frequencies f_1 and f_2 with varying stub length for different fixed stub widths is shown in Fig. 3. As shown in Fig. 3(a), on increasing the stub length (L_s), f_1 and f_2 decrease for any fixed stub width (W_S), however, frequency variation is more for higher stub length values as compared with lower values of stub length. Also, the frequency ratio (f_2/f_1) increases with increasing stub length (L_S) for any fixed stub width (W_S), and for any fixed stub length (L_S) the frequency ratio increases with increasing stub width (W_S) as shown in Fig. 3(b). Therefore, it has been observed that varying stub length and width not only varies the resonant frequencies but the separation between the two frequencies can also be controlled/adjusted as per the required applications by tuning the two parameters, i.e. stub length and width.

Surface current distribution on the antenna

Figure 4 shows the surface current distribution of the dual-band radiating antenna at the two resonant frequencies viz., 60 and 86 GHz. The inclusion of the tuning stub changes the fundamental and higher order mode surface current distribution and thus supports dual resonance at 60 and 86 GHz. As seen in Fig. 4(a), the surface current distribution shows one half wavelength variations along the length of the patch, however, along with the width there is no change in the direction of current distribution. This signifies fundamental mode: TM10 propagation at 60 GHz resonant frequency. Furthermore, from Fig. 4(b), the surface current distribution shows one-half wavelength variation along the patch length as well as along the patch width. This signifies higher order mode: TM11 propagation at 86 GHz resonant frequency. By varying the tuning stub length and width, the current distribution in the stub and the patch can be varied so as to excite a different pair of resonant frequencies.

MMW antenna fabrication

Antenna fabrication at MMW is quite challenging. Accurate fabrication as per simulated dimensions is vital in order to provide accurate characterization of antenna *S*-parameters and radiation pattern. Here, the MMW antenna was fabricated using Printed Circuit Board technology. Due to the simplicity of the proposed structure no complexity or extra fabrication step was introduced while following standard fabrication procedure. For example, slot, a multilayer of patches, coupling alignment, via hole, shorting etc. were deliberately avoided in order to make the fabrication easy. Substrate of Rogers RT5880: $\varepsilon_r = 2.2$, $H = 5$ mils, tan $\delta = 0.002$, metallization (t) = 0.017 mm have been used for realization of MMW antenna prototypes in order to keep the operating frequency well below the safe limit of the substrate and without

https://doi.org/10.1017/S1759078718001009 Published online by Cambridge University Press

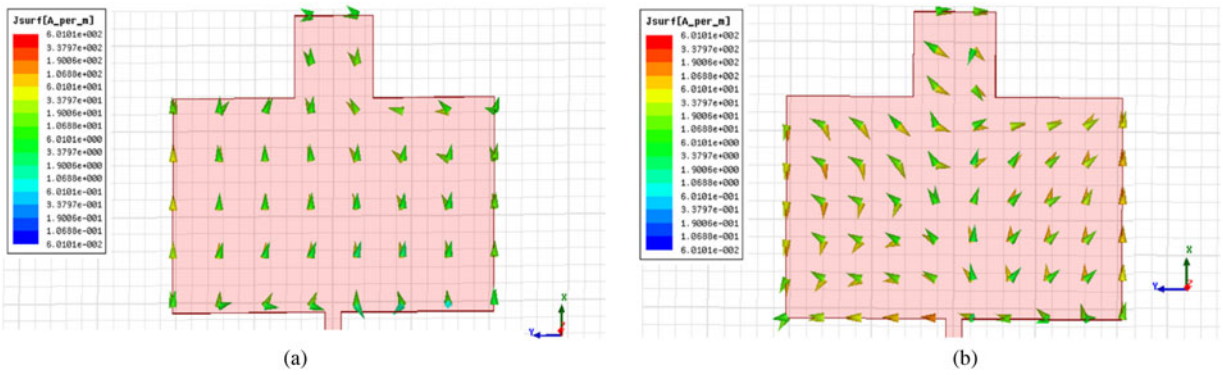

Fig. 4. Surface current distribution for dual-band MMW antenna at: (a) 60 GHz and (b) 86 GHz.

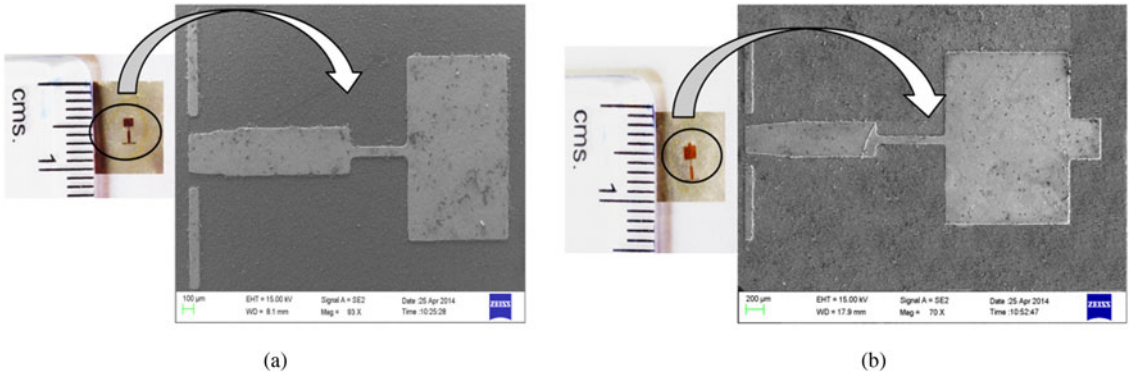

Fig. 5. Fabricated prototypes of designed millimeter wave antennas and their SEM images: (a) Single frequency (94 GHz) (93×-zoom SEM) and (b) Dual frequency (70×-zoom SEM).

exciting higher order mode as given by equation (1). Substrate dimension was $SL \times SW = 5$ mm $\times 5$ mm. The proposed antennas were fabricated as per the dimensions in Table 1. The actual photographs of fabricated antenna prototypes and their scanning electron microscopy (SEM) images are shown in Figs 5(a) and 5(b) for single- and dual-frequency antennas, respectively.

Antenna measurement setup

In order to characterize the fabricated MMW antenna performance, a measurement setup is needed to be designed. An RF probe has been used in order to avoid any interconnection problem between antenna under test (AUT) and the measurement setup. Via hole has been avoided to reduce any measurement error. Use of RF probe is advantages due to its reusability and ease to provide proper contact with AUT as compared with coaxial connectors that are much more expensive and difficult to connect due to the much lower dimensions at MMW. For antenna characterization the two-step calibration process adopted is as follows:

GSG probe calibration

This is done by the similar standard short open load through calibration as done at microwave frequency. However, at the MMW frequency it is done through on wafer open, short, and load provided by the probe supplier.

Gain calibration

This is done by a known standard gain horn antenna. However, at the MMW frequency, losses incurred through probe may affect the gain values hence, extreme care should be taken while gain calibration of the probe tip. Also, the effects of parasitic radiations from the probe tip and energy scattered from metallic portions of the probe station should be taken into account while on-chip antenna gain and radiation pattern measurements.

The gain of AUT has been found using the Friss power transmission equation:

$$\frac{P_r}{P_t} = |S_{21}|^2 = G_t G_r \left(\frac{\lambda}{4\pi R}\right)^2. \quad (7)$$

Here, G_t and G_r are gains of transmitting and receiving antennas, respectively. P_t is the transmitted power, P_r is the received power, R is the distance between AUT and standard horn, and λ is the wavelength of interest.

Results and discussion

Figure 6(a) shows the comparative (measured versus simulated) reflection coefficient plot of the single-frequency MMW antenna prototype. The measured resonant frequency comes out to be $f =$ 93.5 GHz having $S_{11} = -28.5$ dB. The 10 dB fractional bandwidth comes out to be 11.27% (88.3 to 98.6 GHz). Figure 7(a) shows the

https://doi.org/10.1017/S1759078718001009 Published online by Cambridge University Press

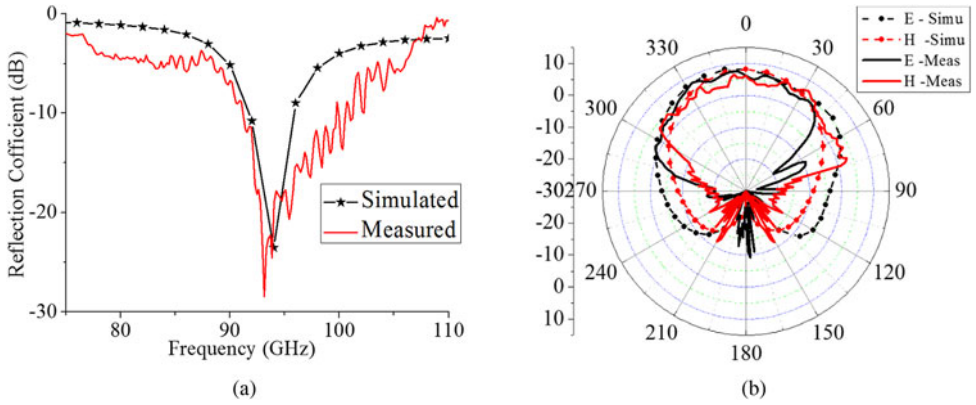

Fig. 6. Comparative (measured versus simulated) plot showing single-frequency (94 GHz) MMW microstrip antenna results: (a) reflection coefficient versus frequency and (b) radiation pattern (*E* and *H* planes) plot at the resonant frequency.

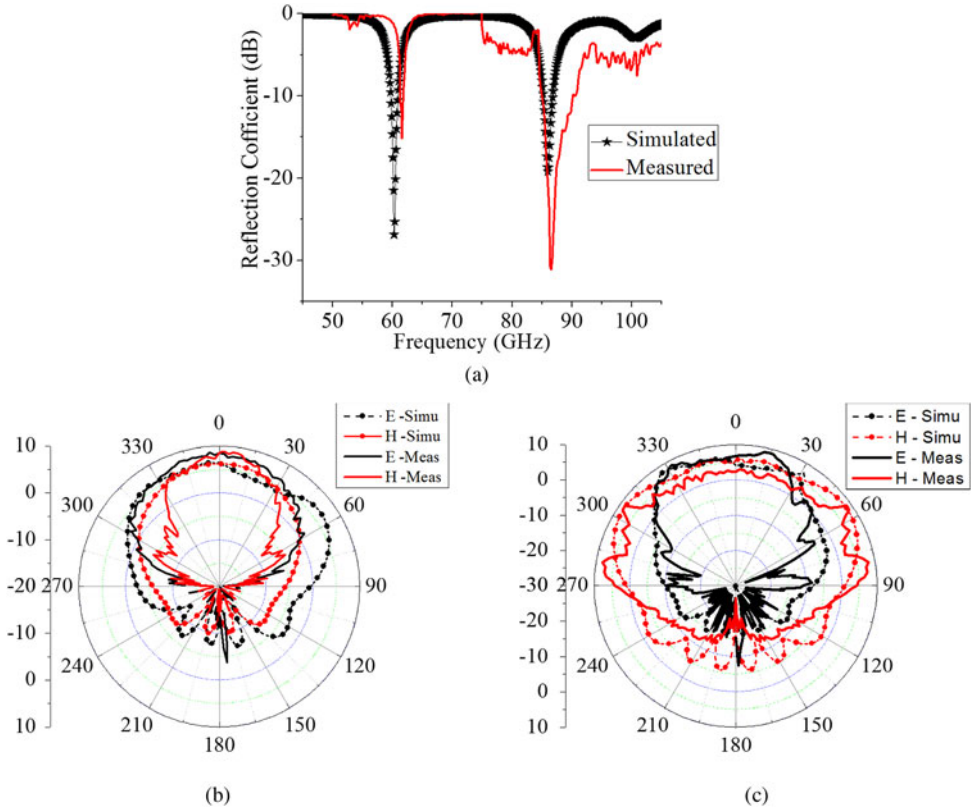

Fig. 7. Comparative (measured versus simulated) plot showing dual-band (60/86 GHz) MMW antenna results for (a) reflection coefficient versus frequency, and radiation pattern at (b) 60 GHz (*E* and *H* planes) and (c) 86 GHz (*E* & *H* planes).

Table 2. Simulated and measured results of designed single- and dual-band MMW antennas

	Frequency (GHz)		*E*-plane gain (dBi)		*H*-plane gain (dBi)	
	Simulated	Measured	Simulated	Measured	Simulated	Measured
Single-freq. antenna	94	93.5	8.09	6.17	8.09	6.2
Dual-freq. antenna	60	60.8	6.5	7.29	6.25	7.36
	86	86.3	7.6	8.73	7.46	8.68

https://doi.org/10.1017/S1759078718001009 Published online by Cambridge University Press

Table 3. Comparison of reported MMW antenna works and the proposed antenna

Reference	Frequency (GHz)	Dual band	Substrate	Technology	B.W (%)	Gain (dBi)	Fabrication complexity	Size (mm^2)
[11]	24/60	Yes	0.13-µm CMOS	On-chip antenna	0.75/1.67	−9/1	Complex	0.76 × 1.045
[10]	41/52.2	Yes	DuPont 951 $\varepsilon_r = 7.4$	SRR	2/–	3.8/4.2	Moderate	–
[9]	60/77	Yes	Silicon	MEMS	–	3.5/4.8	Complex	4.6
[8]	58/77	Yes	CMOS and glass	CMOS and integrated passive device with flip-chip technology	6.1/5.8	−2/0.3	Complex	14
[27]	92	No	GaAs	Circular slot with shorting stub	20/–	3.05/–	Moderate	–
[28]	33.75/36.75	Yes	GaAs	Multilayer, spur-line patch	0.45/0.55	–	Complex	–
[29]	94	No	RT Duroid 5880	Slot-coupled stacked patch horn	30/–	5.5/–	Complex	–
[2]	20.4/30.2	Yes	$\varepsilon_r = 2.55$	Multi-layer frequency selective surface reflectarray	8.4/10.3	–	Complex	–
[30]	5.8/30	Yes	$\varepsilon_{r1} = 2.33$, $\varepsilon_{r2} = 2.2$	Aperture coupled annular ring and substrate-integrated waveguide slot	2.8/6.4	10.2/8	Complex	–
This Work	60/86	Yes	RT Duroid 5880	Stub	2/6.4	7.3/8.7	Simple	3.7

reflection coefficient plot of the dual-band MMW antenna showing measured dual resonance at $f_1 = 60.8$ GHz and $f_2 = 86.3$ GHz with S_{11}: −17.4 dB and −32.1 dB at the two respective resonant frequencies. There is a slight shift in measured and simulated resonant frequencies viz. 0.5% for the 94 GHz single-frequency antenna and 2.1, 1.5% corresponding to 60, 86 GHz. This shift can be accounted for fabrication error, imperfect contact of probe pins to CPW feed-line and parasitic impedance at the feeding point caused due to the three-point GSG probe [27].

Figures 6(b), 7(b), and 7(c) show radiation pattern plots of single- and dual-frequency antennas, respectively in *E*- and *H*-planes. The fabricated single-frequency antenna at 93.5 GHz shows a maximum gain in *E* (*H*) plane = 6.17 dBi (6.2 dBi) at theta = 0°. The dual-frequency MMW antenna prototype at $f_1 = 60.8$ GHz shows a maximum gain of *E* (*H*) plane = 7.29 dBi (7.36 dBi) in the broadside direction (theta = 0°) and at $f_2 = 86.3$ GHz it shows a maximum gain of *E* (*H*) plane = 8.73 dBi (8.68 dBi) at theta = 15°, respectively. The simulated radiation efficiency of the single-frequency antenna is 98.5% and of the dual frequency, MMW antenna is 84.3 and 96.2% for 60 GHz and 86 GHz, respectively.

Here, the measured gain value of the dual-band MMW antenna is higher than simulated which can be accredited to the in-phase reflections from the metallic chuck over which AUT was placed (Table 2).

Thus, from these results, it can be inferred that the proposed antenna operates very well as a concurrent dual-frequency antenna with a very good interband rejection and appreciably good gain as compared with commonly reported MMW dual-band antenna techniques as shown in Table 3. Furthermore, the antenna design is kept simple to achieve the objective of fabrication simplicity and cost efficiency which is very much needed for its commercial applications with concurrent multi-gigabit wireless communication systems at 60 GHz (V band) and 71–88 GHz (E band).

Conclusion

The use of the MMW spectrum has grown tremendously with rising demand for affordable, compact communication systems, higher data rate and spectrum unavailability at microwave frequency. Here, a MMW CPW-fed concurrent dual-band (60/86 GHz) antenna along with measured results of the fabricated prototype has been proposed. The measured results show a maximum gain of around 7.3 and 8.7 dBi at the two respective dual-band resonant frequencies, i.e. 60.8 and 86.3 GHz. Furthermore, the structure is simple, compact, easily integrable with monolithic microwave integrated circuit, and cost-effective. In MMW systems, CPWs are preferred as the interconnecting lines between different modules because of ease of connection and fabrication simplicity. Printed antennas are easily compatible with CPW lines and thus were used in compact MMW frontend design as a low-cost solution. Furthermore, the proposed dual-band MMW antenna structure provides an easy approach for dual-band array antenna implementation at MMW.

Acknowledgement. The authors are very much thankful to Professor Werner Wiesbeck, Karlsruhe Institute of Technology (KIT), Germany for providing fabrication and measurement facility.

References

1. **Marcus M and Pattan B** (2005) Millimeter wave propagation; spectrum management implications. *IEEE Microwave Magazine* **6**, 54–62.

https://doi.org/10.1017/S1759078718001009 Published online by Cambridge University Press

2. **Deng R, Yang F, Xu S and Li M** (2017) An FSS-backed 20/30-GHz dual-band circularly polarized reflectarray with suppressed mutual coupling and enhanced performance. *IEEE Transactions on Antennas and Propagation* **65**, 926–931.
3. **Burasa P, Djerafi T, Constantin NG and Wu K** (2017) On-chip dual-band rectangular slot antenna for single-chip millimeter-wave identification tag in standard CMOS technology. *IEEE Transactions on Antennas and Propagation* **65**, 3858–3868.
4. **Daniels RC and Heath RW** (2007) 60 GHz wireless communications: emerging requirements and design recommendations. *IEEE Vehicular Technology Magazine* **2**, 41–50.
5. **Maci S and Gentili GB** (1997) Dual-frequency patch antennas. *IEEE Antennas and Propagation Magazine* **39**, 13–20.
6. **Wen-Chung L, Chao-Ming W and Yen-Jui T** (2011) Parasitically loaded CPW-fed monopole antenna for broadband operation. *IEEE Transactions on Antennas and Propagation* **59**, 2415–2419.
7. **Li Y and Feng Q** (2013) A compact tri-band monopole antenna with metamaterial loaded for WLAN/WiMAX applications. *Journal of Electromagnetic Waves and Applications* **27**, 772–782.
8. **Ta-Yeh L, Tsenchieh C and Da-Chiang C** (2014) Design of dual-band millimeter-wave antenna-in-package using flip-chip assembly. *IEEE Transactions on Components, Packaging and Manufacturing Technology* **4**, 385–391.
9. **Marnat L, Carreno AAA, Conchouso D, Martinez MG, Foulds IG and Shamim A** (2013) New movable plate for efficient millimeter wave vertical on-chip antenna. *IEEE Transactions on Antennas and Propagation* **61**, 1608–1615.
10. **Kwang IK and Varadan VV** (2010) Electrically small, millimeter wave dual band meta-resonator antennas. *IEEE Transactions on Antennas and Propagation* **58**, 3458–3463.
11. **Jie-Huang HW, Wei J, Yi-Lin C and Jou CF** (2009) A 24/60 GHz dual-band millimeter-wave on-chip monopole antenna fabricated with a 0.13-μm CMOS technology. *IEEE International Workshop on Antenna Technology*, Santa Monica, CA, USA.
12. **Pozar DM** (1983) Considerations for millimeter wave printed antennas. *IEEE Transactions on Antennas and Propagation* **31**, 740–747.
13. **Lin Z and Melde KL** (2006) On-wafer measurement of microstrip-based circuits with a broadband vialess transition. *IEEE Transactions on Advanced Packaging* **29**, 654–659.
14. **Wang Y and Lancaster MJ** (2007) Coplanar to microstrip transitions for on-wafer measurements. *Microwave and Optical Technology Letters* **49**, 100–103.
15. **Vatankhah M, Azarmanesh M and Saghati AP** (2011) A novel broadband CB-CPW to microstrip transition for concept of implementation in RF-circuits. *Journal of Electromagnetic Waves and Applications* **25**, 1817–1827.
16. **Ponchak GE, Tentzeris EM and Katehi LP** (1997) Characterization of finite ground coplanar waveguide with narrow ground planes. *International Journal of Microcircuits and Electronic Packaging* **20**, 167–173.
17. **Schnieder F, Tischler T and Heinrich W** (2003) Modeling dispersion and radiation characteristics of conductor-backed CPW with finite ground width. *IEEE Transactions on Microwave Theory and Techniques* **51**, 137–143.
18. **Tien C-C, Tzuang CKC, Peng ST and Chung-Chi C** (1993) Transmission characteristics of finite-width conductor-backed coplanar waveguide. *IEEE Transactions on Microwave Theory and Techniques* **41**, 1616–1624.
19. **Raskin JP, Gauthier G, Katehi LP and Rebeiz GM** (2000) Mode conversion at GCPW-to-microstrip-line transitions. *IEEE Transactions on Microwave Theory and Techniques* **48**, 158–161.
20. **Balanis CA** (2005) *Antenna Theory: Analysis and Design*. USA: Wiley Interscience.
21. **Richards WF, Davidson S and Long SA** (1985) Dual-band reactively loaded microstrip antenna. *IEEE Transactions on Antennas and Propagation* **33**, 556–561.
22. **Deshmukh AA and Ray KP** (2010) Multi-band configurations of stub-loaded slotted rectangular microstrip antennas. *IEEE Antennas and Propagation Magazine* **52**, 89–103.
23. **Deshpande MD and Bailey MC** (1997) Analysis of stub loaded microstrip patch antennas. *IEEE International Symposium Antennas and Propagation Society*, pp. 610–613.
24. **Deshmukh AA and Ray KP** (2009) Stub loaded multi-band slotted rectangular microstrip antennas. *IET Microwaves, Antennas and Propagation* **3**, 529–535.
25. **Pozar DM** (2004) *Microwave Engineering*. New York: John Wiley & Sons.
26. **Deshmukh AA, Baxi PC, Kamdar VB and Ray KP** (2012) Analysis of stub loaded rectangular microstrip antenna. *IEEE National Conf. Communications, Delhi*.
27. **Anh TH, Han M, Baek YH, Lee SJ, Van HN and Kim JH** (2011) Coplanar waveguide (CPW)-FED circular slot antenna for W-band and imaging system applications. *Microwave and Optical Technology Letters* **53**, 2298–2302.
28. **Hernandez DS, Wang Q, Rezazadeh AA and Robertson ID** (1996) Millimeter-wave dual-band microstrip patch antennas using multilayer GaAs technology. *IEEE Transactions on Microwave Theory and Techniques* **44**, 1590–1593.
29. **Shireen R, Hwang T, Shi S and Prather DW** (2008) Stacked patch excited horn antenna at 94 GHz. *Microwave and Optical Technology Letters* **50**, 2071–2074.
30. **Xiang BJ, Zheng SY, Wong H, Pan YM, Wang KX and Xia MH** (2017) A flexible dual-band antenna with large frequency ratio and different radiation properties over the two bands. *IEEE Transactions on Antennas and Propagation* **66**, 657–667.

Smiriti Agarwal was born in Lucknow, Uttar Pradesh, India. She has received her Ph.D. degree in millimeter wave imaging for target shape and fault identification from the Indian Institute of Technology Roorkee (IIT Roorkee), Roorkee, India. Her research interest includes microwave and millimeter wave active imaging for target identification, non-destructive fault inspection, and millimeter wave planar antenna design. Mrs. Agarwal received a women scientist (WOS-A) fellowship from the Department of Science and Technology (DST) and a research intern fellowship from the Council of Scientific and Industrial Research (CSIR), India. She is currently working as an Assistant Professor at the Department of Electronics and Communication Engineering, G. B. Pant Government Engineering College, New Delhi, India.

Dharmendra Singh was born in Varanasi, Uttar Pradesh, India. He received his Ph.D. degree in electronics engineering from the Institute of Technology (now IIT BHU), Banaras Hindu University, Varanasi, India. Mr. Singh has 20 years of experience in teaching and research. He was a Visiting Scientist Postdoctoral Fellow in the Information Engineering Department, Niigata University, Japan; German Aerospace Center, Cologne, Institute for National Research in Informatics and Automobile, France; Institute of Remote Sensing Applications, Beijing, China; Karlsruhe University, Germany; UPC, Barcelona, and Spain. He is currently a Professor in the Department of Electronics and Communication Engineering, IIT Roorkee, India, and Coordinator Railtel – IIT Roorkee, Centre of Excellence in Telecommunication. He has published more than 200 papers in various journals/conferences. His research interests include microwave absorbers, microwave and optical remote sensing, and microwave imaging.

https://doi.org/10.1017/S1759078718001009 Published online by Cambridge University Press